

Emergence symmetry protected topological phase in spatially tuned measurement-only circuit

Yoshihito Kuno¹ and Ikuo Ichinose^{2*}

¹Graduate School of Engineering Science, Akita University, Akita 010-8502, Japan and

²Department of Applied Physics, Nagoya Institute of Technology, Nagoya, 466-8555, Japan

(Dated: December 27, 2022)

Topological phase transition induced by spatially-tuned single-site measurement is investigated in a measurement-only circuit, in which three different types of projective measurement operator. Specific spatial setting and combination of commutation relations among three measurement operators generate such a transition. In practice, symmetry protected topological (SPT) phase is recovered on even sublattice by eliminating a projective measurement disturbing the SPT via applying another spatially-tuned projective measurement on odd sublattice. We further investigate the critical properties of the phase transition and find that it has the same critical exponents with the two-dimensional percolation transition.

Introduction.— Measurement of quantum many-body system induces nontrivial dynamical effects. One of the most interesting phenomena induced by measurements is entanglement phase transition in hybrid random unitary circuits [1–15]. This phase transition phenomenon appears in various hybrid circuits including a time evolution operators of some many-body Hamiltonian [16–23]. High entanglement of states generated by a unitary time evolution is suppressed by the measurements. Also, as a typical non-equilibrium dynamical aspect, the spread of entanglement or scrambling of the quantum information is suppressed. This change of states on the circuits is not a crossover but phase transition. Interestingly, the criticality of phase transitions in the circuits is mostly classified into a universality class, such as two-dimensional (2D) percolation [3, 24, 25]. Besides unitary evolution with measurements, measurement-only circuit [26, 27] also displays striking phenomena, i.e., combination of multiple kinds of measurements can induce novel phase transitions and generates non-trivial states such as measurement-only thermal state not exhibiting area law of entanglement entropy [27, 28], symmetry protected topological (SPT) state [29, 30] and topological order [28]. It also gives various interesting critical phenomena of the measurement-induced phase transition. In particular, measurement-only circuit with a specific frustration graph [27, 31], which clarifies network relationship of anti-commutation relation between measurement operators, enhances complexity and non-triviality of resultant steady states. Nevertheless, it exhibits universal behavior at transition points, i.e., various phase transitions in various circuits can be classified into a unique or closely-related universality class [1–4].

In general, various setups of the measurement-only circuit are possible, although only some of them have been explored so far. As one of interesting properties of measurement-only circuits, various combinations of anti-commuting measurement operators can induce unexplored non-trivial phenomena. In this work, we shall study a specific example of such measurement-induced

phenomenon in measurement-only circuits, being motivated by recent studies [27–30].

In this study, a measurement-only circuit with three different types of projective measurements is focused. We show that interplay of the specific setting of location of the measurements and suitable combination of the commutation relations among the three projective measurements induces a topological phase transition, generating SPT states. One of the three projective measurements eliminates the disorder projective measurement, which hinders the SPT, and as a result, the state recovers a specific SPT defined on even sublattice in temporal evolution of the circuit. This mechanism seems simple but is definitely interesting as a clear phase transition to sublattice SPT is observed. After explaining essential ingredients of the mechanism, numerical study shows that this transition belongs to the universality class of the classical 2D percolation. Furthermore, we verify that its criticality is universal, independent of a choice of disorder measurements with or without the symmetries of the SPT. This numerical result indicates that the criticality of the 2D percolation emerges universally in measurement-only circuit transition regardless of the symmetry of operators hindering the SPT, i.e., whether the operators preserve or break the SPT symmetry.

Circuit setting.— We consider a L (=even integer)-site spin system with open boundary conditions and study measurement-only circuits with three different types of projective measurement, $\hat{M}_j^{a,b,e}$, which are defined as

$$\begin{aligned}\hat{M}_j^a &= Z_{2j}X_{2j+1}X_{2j+2}X_{2j+3}Z_{2j+4} \\ \hat{M}_j^b &= X_{2j}Z_{2j+1}X_{2j+2}Z_{2j+3} \\ \hat{M}_j^e &= X_{2j+1},\end{aligned}\tag{1}$$

where $j = 0, 1, \dots, j_{max}^\alpha$ for \hat{M}_j^α ($\alpha = a, b, e$), and $j_{max}^a = L/2 - 3$, $j_{max}^b = L/2 - 2$ and $j_{max}^e = L/2 - 1$. Each set of the three kinds of operators is a stabilizer set, i.e., $[\hat{M}_i^\alpha, \hat{M}_j^\alpha] = 0$ and $(\hat{M}_j^\alpha)^2 = 1$ for $\alpha = a, b, e$. The projective measurement of the stabilizer $\{\hat{M}_j^a\}$ gen-

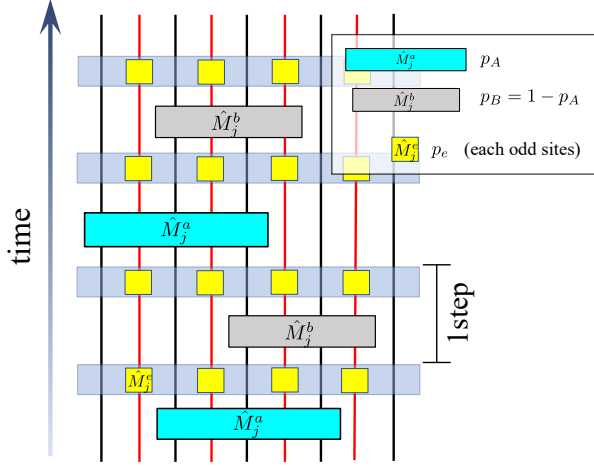


FIG. 1. Schematic figure of measurement only circuit. Black and red line represents even and odd site dynamical lines. Right blue and gray blocks represent projective measurement \hat{M}_j^a and \hat{M}_j^b . Yellow blocks represent projective measurement of \hat{M}_j^e applied only on odd sites.

erates a stable SPT phase with the protection symmetry, $Z_2 \times Z_2$ [32–34] or $Z_2 \times Z_2^T$ [35, 36]. In this work, we focus on the $Z_2 \times Z_2$ symmetry, whose generators are $g_1 \equiv \prod_{i=1}^{L/4} X_{4i}$ and $g_2 \equiv \prod_{i=1}^{L/4} X_{4i+2}$, which commute with $\{\hat{M}_\ell^\alpha\}$, i.e., all of the measurement operators $\{M_j^\alpha\}$ respect the $Z_2 \times Z_2$ symmetry. We note that two sets of $\{\hat{M}_j^a\}$ and $\{\hat{M}_j^b\}$ commute with each other but, some pairs of operators out of $\{\hat{M}_j^b\}$ and $\{\hat{M}_j^e\}$ anti-commute with each other. We shall show shortly that this property derives important consequences for the dynamics of the system as observed from the practical update in the stabilizer numerics [37, 38].

The measurement and time-step process in this circuit are as follows: In each time step, the following two projective measurements are applied. First, we choose \hat{M}^a or \hat{M}^b with probability p_A or $p_B = 1 - p_A$ and choose a measurement site j with uniform probability, and then perform the chosen projective measurement [29, 30]. Second, we apply the \hat{M}_j^e for each j (odd sites from Eq. (1)) with the probability p_e , that is, p_e is a probability density. Please notice the difference between the meaning of the probabilities $p_{A/B}$ and p_e . Single time-step process (the unit of time) consists of the above two successive measurements.

In addition, we comment that, in the present setup, the projective measurement \hat{M}_j^e can be regarded as error emerging only on odd sites with the probability p_e . On the other hand, the other two types of measurements $\hat{M}_j^{a(b)}$ can be regarded as a syndrome and a disorder measurement disturbing the syndrome measurement in error correction literature, respectively.

Intuitive picture of elimination of \hat{M}_j^b .— We can ob-

serve an essential mechanism for eliminating the disorder measurement \hat{M}_j^b . Assuming that, for simplicity, system is periodic and the initial state in the bulk is prepared by the stabilizer sets of $\{\hat{M}_j^a\}$ and $\{\hat{M}_j^e\}$ (See Supplemental Material [39]), then we apply a single measurement of the disorder operator at site j_0 , $\hat{M}_{j_0}^b$, in the bulk. This operation destroys local SPT by $X_{2j_0}Z_{2j_0+1}X_{2j_0+2}Z_{2j_0+3}$. Then, we further perform the measurement $\hat{M}_{j_0}^e = X_{2j_0+1}$. This process is described by an update flow on a check matrix form in the stabilizer formalism as shown in Refs. [37, 38];

$$\begin{aligned}
 & \begin{pmatrix} \vdots \\ X_1 \\ Z_2 X_3 X_4 X_5 Z_6 \\ X_3 \\ Z_4 X_5 X_6 X_7 Z_8 \\ X_5 \\ \vdots \end{pmatrix} \xrightarrow{\text{Measure } \hat{M}_{j_0}^b} \begin{pmatrix} \vdots \\ X_1 \\ X_2 Z_3 X_4 Z_5 \\ Z_2 I_3 X_4 X_5 Z_6 \\ Z_4 X_5 X_6 X_7 Z_8 \\ Z_2 X_3 X_4 I_5 Z_6 \\ \vdots \end{pmatrix} \\
 & \xrightarrow{\text{Measure } \hat{M}_{j_0}^e} \begin{pmatrix} \vdots \\ X_1 \\ X_3 \\ Z_2 I_3 X_4 X_5 Z_6 \\ Z_4 X_5 X_6 X_7 Z_8 \\ Z_2 X_3 X_4 I_5 Z_6 \\ \vdots \end{pmatrix} \xrightarrow{!} \begin{pmatrix} \vdots \\ X_1 \\ Z_2 X_3 X_4 X_5 Z_6 \\ X_3 \\ Z_4 X_5 X_6 X_7 Z_8 \\ X_5 \\ \vdots \end{pmatrix} \quad (2)
 \end{aligned}$$

Here, the final transformation is only to redefine the stabilizer *generators* in basic transformations of check matrices [40]. From the above update example, the initial bulk SPT order is protected by eliminating effects of the disorder measurement $\hat{M}_{j_0}^b$ by the subsequent measurement $\hat{M}_{j_0}^e$. This simply comes from the combination of the commutation relations, $[\hat{M}_j^a, \hat{M}_j^e] = 0$ and $\{\hat{M}_j^a, \hat{M}_j^e\} = 0$. Spatial location of the measurement of $\hat{M}_{j_0}^e$ is important in the above process.

Based on the above observation on the practical process, in the case that the initial state is specified uniquely by all the operators $\{X_j\}$ ($j = 0, \dots, L-1$) and the circuit satisfies the condition such as $p_A < p_B$, we expect that (I) for $p_e = 0$, the SPT order is not be sustained since the measurement \hat{M}_j^b strongly disturbs it, (II) for a sufficiently large p_e , the measurement \hat{M}_j^e can eliminate the effects of the disorder measurement \hat{M}_j^b and the SPT re-emerges. How the SPT is generated (or sustained) by increasing p_e and whether a phase transition takes place at a finite critical probability p_e (denoted by p_e^c) are non-trivial problem. In what follows, we shall clarify these issues by numerical approach.

Observables and numerical approach.— The measurement-only circuit can be simulated efficiently by using the algorithm of the stabilizer circuit for large system sizes [37, 38]. In what follows, we fix $p_A = 0.3$

and $p_B = 0.7$ and vary p_e as a controllable parameter. The initial states are prepared by applying the full elements of $\{X_j\}$.

To capture dynamics of the system, we observe entanglement behavior of the system. Here, in the stabilizer formalism, entanglement entropy for a subsystem X is given by [41, 42], $S_X = n_X - \text{rank}|M_X|$, where n_X is system size of the subsystem X and $\text{rank}|M_X|$ is the number of linear-independent stabilizers defined within the subsystem X [43]. Then, by partitioning the system into four subsystems as shown in Fig. 2(a), we introduce topological entanglement entropy [44, 45]

$$S_t = S_{AB} + S_{BC} - S_A - S_{ABC}.$$

System with the exact SPT order has $S_t = 2$, which is nothing but the number of the generator of $Z_2 \times Z_2$ transformation, corresponding to the logical operators of the system under open boundary conditions. In our target case with probability $p_A = 0.3$, $p_B = 0.7$ and $p_e = 0$, $Z_2 \times Z_2$ SPT state does *not* appear as a steady state, since sufficiently frequent measurement of \hat{M}_j^b destroys the SPT, and then, the saturation value of S_t is much smaller than 2.

For the numerical calculation for the target observables, we employ 800 – 1000 different measurement patterns for various system sizes and various values of p_e , and take an ensemble average of saturation value of the observables at $t_N = 10L$, where the state is expected to reach a steady state.

Scaling analysis of phase transition induced by single spatially-fixed error. — We calculate averages of the saturation values of S_t denoted by $\langle S_t \rangle$ as a function of p_e for various system sizes. The results are shown in Fig. 2(b). The data indicate the existence of a phase transition since all data obtained for various system sizes cross with each other at a single point.

To detect the phase transition point and examine its criticality, we employ the finite-size scaling (FSS) analysis for $\langle S_t \rangle$. Here, we assume the following scaling ansatz,

$$\langle S_t \rangle(p_e, L) = \Psi((p_e - p_e^c)L^\nu),$$

where Ψ is a scaling function, ν is the critical exponent of a typical length and p_e^c is the critical measurement probability for \hat{M}_j^b . In the FSS, we determine the scaling function Ψ , by using the fitting methods of the FSS; the fitting curve for the scaling function is obtained via a 10-th order polynomial function with the best optimal coefficients for various values of p_e and ν , and then the coefficient of determination R^2 is estimated. The R^2 quantifies how accurately the values of $\langle S_t \rangle$ with different system sizes collapse to a single curve. Similar procedure was previously employed to study phase-transition properties in similar measurement-only circuits and obtained reliable results [29, 30].

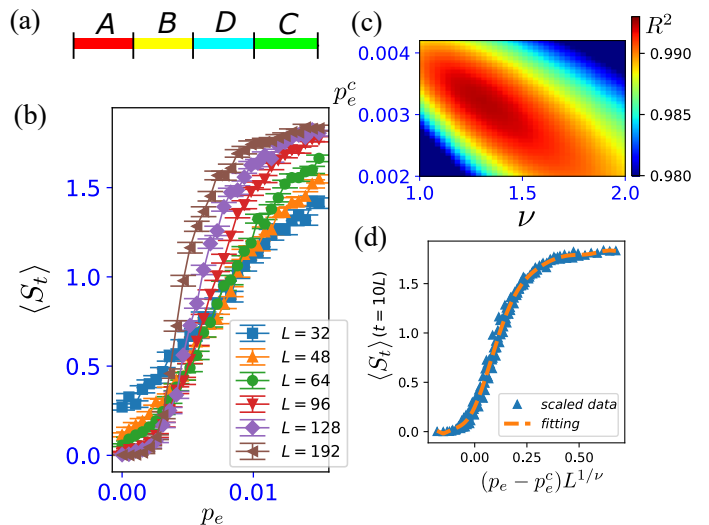


FIG. 2. (a) The system partition for the calculation of the topological entanglement entropy, S_t . Each four subsystem has $L/4$ lattice sites. (b) Saturation values as increasing p_e for different system sizes. The values are those at $t_N = 10L$. (c) R^2 distribution on ν - p_e plane. The optimal values are $R^2 = 0.992(4)$, $\nu = 1.30(0)$ and $p_e^c = 0.00315(5)$. (d) The scaling fitting function and scaled data set for $\nu = 1.30(0)$ and $p_e^c = 0.00315(5)$. The scaling fitting function is 10-th degree polynomial function. For all data, we set $p_A = 0.3$, $p_B = 0.7$.

The FSS result is displayed in Figs. 2(c) and 2(d), obtained from the $L = 48 - 192$ data. The critical transition rate is estimated as $p_e^c = 0.00315(5)$ and the exponent $\nu = 1.30(0)$. The obtained value of ν is significantly close to that of the 2D percolation $\nu = 4/3$, which has been reported in similar SPT phase transitions in measurement-only circuits [29, 30]. This result indicates that the present circuit including elimination process of the disorder projective measurement $\{\hat{M}_j^b\}$ belongs to the same universality class of these systems.

In the above, we studied the topological entanglement entropy S_t to observe the SPT-ordered states. To verify and support the existence of the SPT in the bulk, we measure the *even-site only* Edward-Anderson type of string topological order parameter (STO) [29], which is defined as follows,

$$|\text{STO}|^2 = |\langle \psi(t) | G^s(i_0, j_0) | \psi(t) \rangle|^2,$$

where $|\psi(t)\rangle$ is a unique stabilizer state at a time t , i.e., $s^\ell(t)|\psi(t)\rangle = |\psi(t)\rangle$ [$\{s^\ell\}$ is the stabilizer set at t], and

$$G^s(i_0, j_0) = Z_{2i_0} Y_{2(i_0+1)} \left(\prod_{i_0+2}^{j_0-2} X_{2k} \right) Y_{2(j_0-1)} Z_{2j_0}.$$

The practical calculation scheme in numerics is explained in Supplemental Material [39]. Figure 3 shows the result

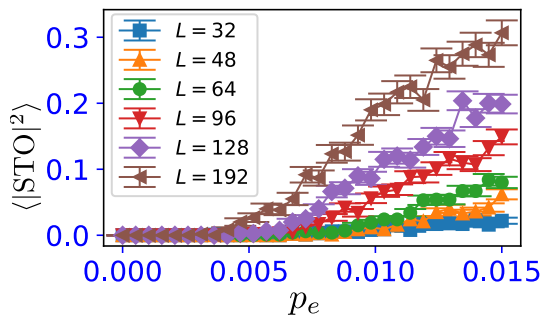


FIG. 3. Behavior of saturation values of the string topological order (STO) in the bulk. For all data, we set $p_A = 0.3$ and $p_B = 0.7$, $i_0 = 2$ and $j_0 = L/2 - 3$ for the calculation of the STO.

of the averaged saturation values of STO, $\langle |\text{STO}|^2 \rangle$, sampled at $t_N = 10L$ as a function of p_e for various system sizes. The numerical results indicate that the averaged STO for large systems with large p_e exhibit sufficiently large values, i.e., giving a clear evidence for the existence of the bulk SPT order and phase transition in the bulk, in contrast to the claim in a similar calculation in Ref.[29].

We observe that the STO is an increasing function of p_e for all system sizes, which is a signal of the existence of the SPT in the bulk defined on even sites. We further carry out the FSS for the STO and the obtained results are shown in Supplemental Material [39]. The estimated values of p_e^c and ν are fairly close to those obtained by the FSS of S_t . We expect that the FSS of $\langle S_t \rangle$ is more reliable than that of the STO as the R^2 -analysis indicates.

Symmetry breaking type measurement \hat{M}_j^d .— We investigate effects by a different type of measurement operator instead of $\{\hat{M}_j^b\}$. Here, as a specific example, we consider

$$\hat{M}_j^d = Z_{2j}Z_{2j+1}Z_{2j+2}Z_{2j+3}Z_{2j+4}, \quad (3)$$

where $j = 0, 1, \dots, j_{max}^b$ and $j_{max}^b = L/2 - 3$. $\{\hat{M}_j^d\}$ is a stabilizer set, i.e., $[\hat{M}_i^d, \hat{M}_j^d] = 0$, and $(\hat{M}_j^d)^2 = 1$. They satisfy the same commutation relations with the former set of measurement operators, i.e., the two sets of $\{\hat{M}_j^a\}$ and $\{\hat{M}_j^e\}$ commute with each other, but certain pairs out of two sets of $\{\hat{M}_j^d\}$ and $\{\hat{M}_j^e\}$ anti-commute.

The $\{\hat{M}_j^d\}$ projective measurement operators, however, do *not* respect the $Z_2 \times Z_2$ symmetry. Thus, these projective operators strongly suppress the emergence of the $Z_2 \times Z_2$ SPT phase even for small $p_D = 1 - p_A$ and $p_e = 0$ since the topological entanglement entropy S_t vanishes due to the symmetry breaking effects. Under this situation, we carry out similar calculations as in Fig. 2. The results are shown in Fig. 4.

We also observe an elimination transition similar to the former case as shown in Fig. 4(a) with the FSS analysis summarized in Figs. 4(b) and 4(c). From the FSS of $L = 48 - 192$ data, the critical transition rate and expo-

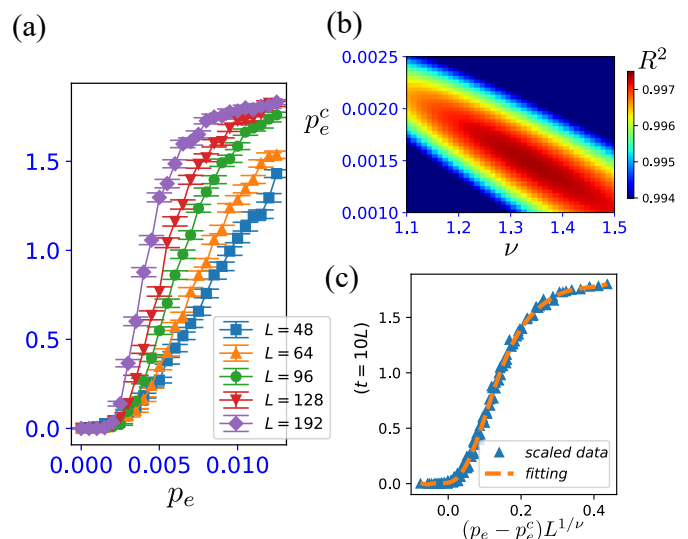


FIG. 4. (a) Saturation values as a function of p_e for various system sizes. The values are those at $t_N = 10L$. (b) R^2 distribution on ν - p_e^c plane. The optimal values are $R^2 = 0.997(8)$, $\nu = 1.36(2)$ and $p_e^c = 0.00152(2)$. (c) The scaling fitting function and scaled data set for $\nu = 1.36(2)$ and $p_e^c = 0.00152(2)$. The scaling fitting function is 10-th degree polynomial function. For all data, we set $p_A = 0.3$, $p_B = 0.7$.

nent are estimated as $p_e^c = 0.00152(2)$ and $\nu = 1.36(2)$. This value of ν is substantially close to the 2D percolation $\nu = 4/3$ as in the former case. Therefore, the numerics of this case indicates that even for finite probability rate of $\{\hat{M}_j^d\}$ that breaks the $Z_2 \times Z_2$ symmetry, the symmetry breaking effect is also eliminated by the projective measurement $\{\hat{M}_j^e\}$ for sufficiently large p_e , and the $Z_2 \times Z_2$ SPT order appears as a steady state. Thus, the numerical result in this work indicates that the 2D percolation picture is fairly universal at the criticality of phase transitions generating SPT steady states.

Conclusion.— Specific spatial setting and combination of commutation relations among three measurement operators induce a novel type of topological phase transition in a measurement-only circuit, where the steady state has a SPT order defined on sublattice only. This SPT is recovered by eliminating a projective measurement suppressing the SPT order. This elimination process is simple, but spatially well-located measurement induces a clear measurement-only phase transition, not a crossover. The detailed analysis of criticality exhibits robustness of the 2D percolation universality class at the criticality of phase transitions generating of SPT steady states. We expect that various spatially-tuned measurements with various kinds of projective operators induce a rich non-trivial phase transition in measurement-only circuits.

Acknowledgements.— This work is supported by JSPS KAKEN-HI Grant Number JP21K13849 (Y.K.).

-
- * A professor emeritus
- [1] Y. Li, X. Chen, and M. P. A. Fisher, Quantum zeno effect and the many-body entanglement transition, *Phys. Rev. B* **98**, 205136 (2018).
 - [2] B. Skinner, J. Ruhman, and A. Nahum, Measurement-induced phase transitions in the dynamics of entanglement, *Phys. Rev. X* **9**, 031009 (2019).
 - [3] Y. Li, X. Chen, and M. P. A. Fisher, Measurement-driven entanglement transition in hybrid quantum circuits, *Phys. Rev. B* **100**, 134306 (2019).
 - [4] R. Vasseur, A. C. Potter, Y.-Z. You, and A. W. W. Ludwig, Entanglement transitions from holographic random tensor networks, *Phys. Rev. B* **100**, 134203 (2019).
 - [5] A. Chan, R. M. Nandkishore, M. Pretko, and G. Smith, Unitary-projective entanglement dynamics, *Phys. Rev. B* **99**, 224307 (2019).
 - [6] M. Szyniszewski, A. Romito, and H. Schomerus, Entanglement transition from variable-strength weak measurements, *Phys. Rev. B* **100**, 064204 (2019).
 - [7] S. Choi, Y. Bao, X.-L. Qi, and E. Altman, Quantum error correction in scrambling dynamics and measurement-induced phase transition, *Phys. Rev. Lett.* **125**, 030505 (2020).
 - [8] Y. Bao, S. Choi, and E. Altman, Theory of the phase transition in random unitary circuits with measurements, *Phys. Rev. B* **101**, 104301 (2020).
 - [9] C.-M. Jian, Y.-Z. You, R. Vasseur, and A. W. W. Ludwig, Measurement-induced criticality in random quantum circuits, *Phys. Rev. B* **101**, 104302 (2020).
 - [10] S. Vijay, [Measurement-driven phase transition within a volume-law entangled phase](#) (2020).
 - [11] S. Sang and T. H. Hsieh, Measurement-protected quantum phases, *Phys. Rev. Res.* **3**, 023200 (2021).
 - [12] S. Sang, Y. Li, T. Zhou, X. Chen, T. H. Hsieh, and M. P. Fisher, Entanglement negativity at measurement-induced criticality, *PRX Quantum* **2**, 030313 (2021).
 - [13] A. Nahum, S. Roy, B. Skinner, and J. Ruhman, Measurement and entanglement phase transitions in all-to-all quantum circuits, on quantum trees, and in landau-ginsburg theory, *PRX Quantum* **2**, 010352 (2021).
 - [14] T. Hashizume, G. Bentsen, and A. J. Daley, Measurement-induced phase transitions in sparse nonlocal scramblers, *Phys. Rev. Res.* **4**, 013174 (2022).
 - [15] M. P. A. Fisher, V. Khemani, A. Nahum, and S. Vijay, Random quantum circuits [10.48550/ARXIV.2207.14280](#) (2022).
 - [16] Y. Fuji and Y. Ashida, Measurement-induced quantum criticality under continuous monitoring, *Phys. Rev. B* **102**, 054302 (2020).
 - [17] S. Goto and I. Danshita, Measurement-induced transitions of the entanglement scaling law in ultracold gases with controllable dissipation, *Phys. Rev. A* **102**, 033316 (2020).
 - [18] Q. Tang and W. Zhu, Measurement-induced phase transition: A case study in the nonintegrable model by density-matrix renormalization group calculations, *Phys. Rev. Res.* **2**, 013022 (2020).
 - [19] O. Lunt and A. Pal, Measurement-induced entanglement transitions in many-body localized systems, *Phys. Rev. Res.* **2**, 043072 (2020).
 - [20] X. Turkeshi, A. Biella, R. Fazio, M. Dalmonte, and M. Schiró, Measurement-induced entanglement transitions in the quantum ising chain: From infinite to zero clicks, *Phys. Rev. B* **103**, 224210 (2021).
 - [21] G. Kells, D. Meidan, and A. Romito, Topological transitions with continuously monitored free fermions [10.48550/ARXIV.2112.09787](#) (2021).
 - [22] C. Fleckenstein, A. Zorzato, D. Varjas, E. J. Bergholtz, J. H. Bardarson, and A. Tiwari, Non-hermitian topology in monitored quantum circuits, *Phys. Rev. Res.* **4**, L032026 (2022).
 - [23] Y. Kuno, T. Orito, and I. Ichinose, Purification and scrambling in a chaotic hamiltonian dynamics with measurements, *Phys. Rev. B* **106**, 214304 (2022).
 - [24] A. Zabalo, M. J. Gullans, J. H. Wilson, S. Gopalakrishnan, D. A. Huse, and J. H. Pixley, Critical properties of the measurement-induced transition in random quantum circuits, *Phys. Rev. B* **101**, 060301 (2020).
 - [25] S. Sharma, X. Turkeshi, R. Fazio, and M. Dalmonte, Measurement-induced criticality in extended and long-range unitary circuits, *SciPost Phys. Core* **5**, 023 (2022).
 - [26] N. Lang and H. P. Büchler, Entanglement transition in the projective transverse field ising model, *Phys. Rev. B* **102**, 094204 (2020).
 - [27] M. Ippoliti, M. J. Gullans, S. Gopalakrishnan, D. A. Huse, and V. Khemani, Entanglement phase transitions in measurement-only dynamics, *Phys. Rev. X* **11**, 011030 (2021).
 - [28] A. Lavasani, Y. Alavirad, and M. Barkeshli, Topological order and criticality in $(2 + 1)$ D monitored random quantum circuits, *Phys. Rev. Lett.* **127**, 235701 (2021).
 - [29] A. Lavasani, Y. Alavirad, and M. Barkeshli, Measurement-induced topological entanglement transitions in symmetric random quantum circuits, *Nature Physics* **17**, 342 (2021).
 - [30] K. Klocke and M. Buchhold, Topological order and entanglement dynamics in the measurement-only xxx quantum code, *Phys. Rev. B* **106**, 104307 (2022).
 - [31] A. Chapman and S. T. Flammia, Characterization of solvable spin models via graph invariants, *Quantum* **4**, 278 (2020).
 - [32] W. Son, L. Amico, R. Fazio, A. Hamma, S. Pascazio, and V. Vedral, Quantum phase transition between cluster and antiferromagnetic states, *Europhysics Letters* **95**, 50001 (2011).
 - [33] W. Son, L. Amico, and V. Vedral, Topological order in 1d cluster state protected by symmetry, *Quantum Information Processing* **11**, 1961 (2011).
 - [34] Y. Bahri, R. Vosk, E. Altman, and A. Vishwanath, Localization and topology protected quantum coherence at the edge of hot matter, *Nature Communications* **6**, 7341 (2015).
 - [35] R. Verresen, R. Moessner, and F. Pollmann, One-dimensional symmetry protected topological phases and their transitions, *Phys. Rev. B* **96**, 165124 (2017).
 - [36] A. Smith, B. Jobst, A. G. Green, and F. Pollmann, Crossing a topological phase transition with a quantum computer, *Phys. Rev. Res.* **4**, L022020 (2022).
 - [37] D. Gottesman, The heisenberg representation of quantum computers [10.48550/ARXIV.QUANT-PH/9807006](#) (1998).
 - [38] S. Aaronson and D. Gottesman, Improved simulation of stabilizer circuits, *Phys. Rev. A* **70**, 052328 (2004).
 - [39] Supplemental material: A. Tractable update behavior to SPT for small size system in the limit $p_A = 1$ and

- $p_e = 1$, B. Computation of string topological order and scaling analysis, C. Scaling analysis of the string order.
- [40] M. A. Nielsen and I. L. Chuang, Quantum Computation and Quantum Information (Cambridge University Press, 2000).
 - [41] D. Fattal, T. S. Cubitt, Y. Yamamoto, S. Bravyi, and I. L. Chuang, Entanglement in the stabilizer formalism [10.48550/ARXIV.QUANT-PH/0406168](#) (2004).
 - [42] A. Nahum, J. Ruhman, S. Vijay, and J. Haah, Quantum entanglement growth under random unitary dynamics, [Phys. Rev. X **7**, 031016 \(2017\)](#).
 - [43] $|M_X|$ is a portion of the check matrix, which is composed of vertically stacked vector representations of stabilizer operators represented by each component of the Pauli operator [40]. We calculated the rank of $|M_X|$ by a binary Gaussian elimination.
 - [44] B. Zeng, X. Chen, D.-L. Zhou, and X.-G. Wen, Quantum information meets quantum matter – from quantum entanglement to topological phase in many-body systems [10.48550/ARXIV.1508.02595](#) (2015).
 - [45] B. Zeng and D. L. Zhou, Topological and error-correcting properties for symmetry-protected topological order, [Europhysics Letters **113**, 56001 \(2016\)](#).

SUPPLEMENTAL MATERIAL

A: TRACTABLE UPDATE BEHAVIOR TO SPT FOR SMALL SIZE SYSTEM IN THE LIMIT $p_A = 1$ AND $p_e = 1$.

Let us consider $L = 12$ system with open boundary conditions and start with the initial state specified by the full elements of $\{X_j\}$ ($j = 0, \dots, 11$). The circuit of the limiting $p_A = 1$ case dynamically creates an ideal $Z_2 \times Z_2$ SPT order defined only on the even sublattice, even though the measurement of \hat{M}_j^e does not affect the time evolution of the circuit. By applying measurement of the operator \hat{M}_j^a for a uniform random j many times, the state is obliged to reach the following steady state

$$\begin{array}{ccc}
 \begin{pmatrix} X_0 \\ X_1 \\ X_2 \\ X_3 \\ X_4 \\ X_5 \\ X_6 \\ X_7 \\ X_8 \\ X_9 \\ X_{10} \\ X_{11} \end{pmatrix} & \xrightarrow{\text{Measure all } \hat{M}_j^a} & \begin{pmatrix} \hat{M}_0^a \\ X_2 \\ \hat{M}_1^a \\ X_3 \\ \hat{M}_2^a \\ X_5 \\ \hat{M}_3^a \\ X_7 \\ \hat{M}_4^a \\ X_0 X_4 X_8 \\ X_2 X_6 X_{10} \\ X_{11} \end{pmatrix} \\
 & & \xrightarrow{\text{Pick up even sites}} \begin{pmatrix} Z_0 I_1 X_2 I_3 Z_4 \\ Z_2 I_3 X_4 I_5 Z_6 \\ Z_4 I_5 X_6 I_7 Z_8 \\ Z_6 I_7 X_8 I_9 Z_{10} \\ X_0 X_4 X_8 \\ X_2 X_6 X_{10} \end{pmatrix}. \quad (4)
 \end{array}$$

Here, we focus on the even sites and recognize that the linearly-independent stabilizers are the ones of the $Z_2 \times Z_2$ SPT and the corresponding logical operators. Thus, on the even sublattice, $Z_2 \times Z_2$ SPT state appears. Also, note that the stabilizers of the SPT and logical operators are not affected by the projective measurement of \hat{M}_j^e since these measurements are performed on odd sites.

B: COMPUTATION OF STRING TOPOLOGICAL ORDER AND SCALING ANALYSIS

We briefly explain how to calculate the STO in the numerics. The density matrix of the system (a pure state) is written by

$$\rho(t) = \prod_{\ell=0}^{L-1} \left(\frac{1 + s^\ell(t)}{2} \right),$$

where $s^\ell(t)$ is updated stabilizers at a time t . We calculate the Edward-Anderson grass-like string order

$$|\langle \text{STO} \rangle|^2 = |\langle \psi(t) | G^s | \psi(t) \rangle|^2,$$

where $|\psi(t)\rangle$ is a unique stabilizer state at a time t , $s^\ell(t)|\psi(t)\rangle = |\psi(t)\rangle$ for $\forall \ell$, and

$$G^s(i_0, j_0) = Z_{2i_0} Y_{2(i_0+1)} \left(\prod_{i_0+2}^{j_0-2} X_{2k} \right) Y_{2(j_0-1)} Z_{2j_0}.$$

The STO is calculated in the stabilizer formalism as $G^s(i_0, j_0)$ is only written by Pauli string without imaginary factor i and $(G^s)^2 = 1$. Each stabilizer $s^\ell(t)$ commutes or anti-commutes with G^s at $\forall t$, $s^\ell(t)G^s = \alpha_\pm^\ell G^s s^\ell(t)$ with $\alpha_\pm^\ell = \pm 1$. The STO is reduced to a simple form

$$\begin{aligned}
 |\text{STO}|^2 &= \frac{1}{2^L} \langle \psi(t) | G^s \left(\prod_{\ell=1}^L (1 + s^\ell(t)) \right) G^s | \psi(t) \rangle \\
 &= \frac{1}{2^L} \prod_{\ell=1}^L \langle \psi(t) | (1 + \alpha_\pm^\ell s^\ell(t)) | \psi(t) \rangle \\
 &= \frac{1}{2^L} \prod_{\ell=1}^L (1 + \alpha_\pm^\ell),
 \end{aligned}$$

where we used $G^s(1 + s^\ell(t))G^s = (1 + G^s s^\ell(t)G^s) = (1 + \alpha_\pm^\ell s^\ell(t))$ and $s^\ell(t)|\psi(t)\rangle = |\psi(t)\rangle$ at $\forall t$. For the ideal $Z_2 \times Z_2$ SPT phase, due to $\alpha_\pm^\ell = 1$ for $\forall \ell$, $|\text{STO}|^2 = 1$ while for no $Z_2 \times Z_2$ SPT phase, strictly $|\text{STO}|^2 = 0$ due to due to $\alpha_\pm^\ell = -1$ for $\forall \ell$.

C: SCALING ANALYSIS OF THE STRING ORDER

We show the finite-size scaling (FSS) analysis for the STO defined in the main text. In the FSS, we use the averaged saturation values of the STO, $\langle |\text{STO}|^2 \rangle$, in the same parameter setting ($p_A = 0.3$ and $p_B = 0.7$) and the saturation values are taken at $t = 10L$, as shown in Fig. 3 in the main text. To detect phase transition point of p_e and examine its criticality from the data of the STO in

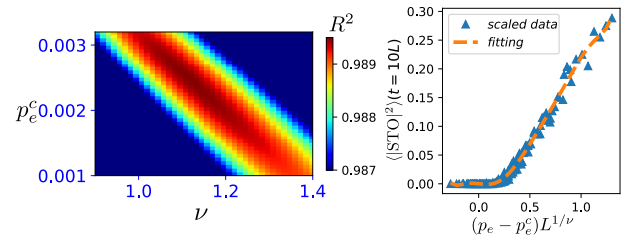


FIG. 5. Scaling analysis of the STO: (Left) R^2 distribution on ν - p_e plane. The optimal values are $R^2 = 0.989(5)$, $\nu = 1.113(5)$ and $p_e^c = 0.00243(1)$. (Right) The scaling fitting function and scaled data set for $\nu = 1.113(5)$ and $p_e^c = 0.00243(1)$. The scaling fitting function is 10-th degree polynomial function. For all data, we set $p_A = 0.3$, $p_B = 0.7$.

the bulk, we carried out the same approach to the main manuscript. Here, we assume a scaling function of the same form to the topological entanglement entropy,

$$\langle |\text{STO}|^2 \rangle(p_e, L) = \Phi((p_e - p_e^c)L^\nu),$$

where Φ is a scaling function and ν is the critical exponent and p_e^c is the critical measurement probability.

The FSS result is summarized in Fig. 5. From the fitting by using $L = 48 - 192$ data, we obtained $R^2 = 0.989(5)$ as the best optimal. The optimal critical transition rate is estimated as $p_e^c = 0.00243(1)$ and the optimal

critical exponent also $\nu = 1.113(5)$. Compared to the FSS results of the topological entanglement entropy in the main text, the values of p_e^c and ν are slightly smaller than those of the topological entanglement entropy, but the estimated value of ν is close to the 2D percolation $\nu = 4/3$. Since the value of R^2 in the FSS of the STO is slightly smaller than that of the topological entanglement entropy, the results of the FSS of the topological entanglement entropy is more reliable.